

FAST SOLVERS FOR THE REYNOLDS EQUATION ON PIECEWISE LINEAR GEOMETRIES

SARAH DENNIS* AND THOMAS G. FAI†

Abstract. The Reynolds equation is derived from the incompressible Navier Stokes equations under the lubrication assumptions of a long and thin domain geometry and a small scaled Reynolds number. The Reynolds equation is an elliptic differential equation and a dramatic simplification from the governing equations. When the fluid domain is piecewise linear, the Reynolds equation has an exact solution that we formulate by coupling the exact solutions of each piecewise component. We consider a formulation specifically for piecewise constant heights, and a more general formulation for piecewise linear heights; in both cases the linear system is inverted using the Schur complement. These methods can also be applied in the case of non-linear heights by approximating the height as piecewise constant or piecewise linear, in which case the methods achieve second order accuracy. We assess the time complexity of the two methods, and determine that the method for piecewise linear heights is linear time for the number of piecewise components. As an application of these methods, we explore the limits of validity for lubrication theory by comparing the solutions of the Reynolds and the Stokes equations for a variety of linear and non-linear textured slider geometries.

1. Introduction. In hydrodynamic theory, the lubrication assumptions of a long thin domain and a small scaled Reynolds number promote a scaling argument in which the inertial velocity and cross-film pressure gradient terms are considered negligible in the Navier-Stokes equations. The resulting Reynolds equation is appealing, providing an elliptic differential equation for pressure which encompasses the incompressibility condition. The Stokes equation similarly arises from the Navier-Stokes equations under the assumption of a zero Reynolds number. The Stokes equation has relaxed restrictions on the ratio of length scales compared to the Reynolds equation, providing a standpoint from which we observe the sensitivity of the Reynolds equation to the thin film condition.

Previous research on the differences between flows modeled by the Reynolds equation and the Stokes equation has highlighted the sensitivity of lubrication theory to variations in the fluid height. In particular, in the limit of zero Reynolds number flows, discrepancies between lubrication theory and Stokes flow increase with both the magnitude and frequency of large gradients in the height [4, 2, 5]. The total pressure drop modeled by the Reynolds equation may be underestimated due to additional pressure losses at points of sudden expansion that are not accurately modeled [6, 5]. Furthermore, notable flow features of corner recirculation seen in Stokes flow are not accurately captured with the Reynolds equation [1, 2, 14]. We consider a variety of textured slider bearings to observe these differences between the solutions of the Reynolds and the Stokes equations.

When the fluid domain has a linear or constant height profile, the Reynolds equation has an exact solution. Approximating the height as piecewise constant or piecewise linear, we couple the exact solutions to the Reynolds equation on each piecewise component using the conditions of constant flux and continuous pressure. The resulting linear system of equations can be efficiently solved using the Schur complement [7], leading to an exact solution for the Reynolds equation in the case of piecewise linear heights, and a second order accurate solution for arbitrary non-linear heights. Compared with a standard finite difference approach, the piecewise analytic

*Department of Mathematics, Brandeis University, Waltham MA (sarahdennis@brandeis.edu)

†Department of Mathematics and Volen Center for Complex Systems, Brandeis University, Waltham MA (tfai@brandeis.edu)

methods are robust, retaining second order accuracy even for discontinuous height profiles. As an application of the methods for the Reynolds equation, we explore the range of validity for lubrication theory by comparing to Stokes flow.

We present two methods of solution for the Reynolds equation: one approach considers a piecewise constant approximation of the fluid domain, and the other considers a more general piecewise linear approximation. A similar approach of piecewise exact solutions to the Reynolds equation is considered in [12]; here, we also assess the performance of the piecewise linear (PWL) and piecewise constant (PWC) methods in approximating the solution for non-linear height functions. We compare the performance of each method for the Reynolds equation in terms of time complexity, including a comparison to a standard finite difference (FD) method; we determine that the PWL method performs fastest, running in linear time for the number of piecewise components.

Finally, to demonstrate the PWL and PWC methods and to examine the range of validity for lubrication theory, we consider four examples of textured sliders: a backward facing step, a wedge slider, a logistic slider, and a sinusoidal slider. We contrast the solutions from the Reynolds equation and the Stokes equation, confirming that large surface gradients cause the lubrication assumptions to break down and correspond to significant discrepancies between lubrication theory and Stokes flows.

Source code is available at <https://github.com/sarah-dennis/Stokes-Reynolds>.

2. Lubrication Theory. The Reynolds equation is derived from the Navier-Stokes equations under the lubrication assumptions [10]. For the two dimensional fluid domain $(x, y) \in [x_0, x_N] \times [0, h(x)]$, denote the characteristic length scales $L_x = x_N - x_0$ and $L_y = \max h(x) > 0$, and the length scale ratio $\varepsilon = L_y/L_x$. Given a prescribed constant flux $Q \neq 0$, the characteristic fluid velocities are given by $U_* = Q/L_y$ and $V_* = Q/L_x$. The Reynolds number is given by $\text{Re} = \rho U_* L_x / \eta$ where η is the constant dynamic viscosity ($\eta = 1$) and ρ is the constant density ($\rho = 1$). The lubrication assumptions $\varepsilon \ll 1$ and $\varepsilon^2 \text{Re} \ll 1$ characterize a long and thin fluid with a small scaled Reynolds number; these assumptions yield an approximation to the Navier-Stokes equations (C.2) and (C.3), resulting in the momentum equations,

$$(2.1) \quad \frac{\partial p}{\partial x} = \eta \frac{\partial^2 u}{\partial y^2},$$

$$(2.2) \quad \frac{\partial p}{\partial y} = 0.$$

Together with incompressibility,

$$(2.3) \quad \frac{\partial u}{\partial x} + \frac{\partial v}{\partial y} = 0,$$

(2.1) and (2.2) constitute the governing equations for lubrication theory.

We assume the no-slip boundary condition at the fluid-surface interfaces $y = 0$ and $y = h(x)$. Without loss of generality, the velocity boundary conditions are,

$$(2.4) \quad u(x, 0) = \mathcal{U} \quad u(x, h(x)) = 0,$$

$$(2.5) \quad v(x, 0) = 0 \quad v(x, h(x)) = 0.$$

The velocity $u(x, y)$ is determined through integration of (2.1) and applying the boundary conditions (2.4),

$$(2.6) \quad u(x, y) = \frac{1}{2\eta} \frac{dp}{dx} (y^2 - h(x)y) + \frac{\mathcal{U}}{h(x)} (h(x) - y).$$

The velocity $v(x, y)$ is then determined from incompressibility (2.3) and applying the boundary conditions (2.5),

$$(2.7) \quad v(x, y) = \frac{-1}{6\eta} \frac{d^2 p}{dx^2} y^3 + \frac{1}{2} \left(\frac{1}{2\eta} \left(\frac{d^2 p}{dx^2} h(x) + \frac{dp}{dx} \frac{dh}{dx} \right) - \frac{\mathcal{U}}{[h(x)]^2} \frac{dh}{dx} \right) y^2.$$

From incompressibility, the condition of constant flux \mathcal{Q} ,

$$(2.8) \quad \mathcal{Q} = \int_0^{h(x)} u(x, y) dy = \frac{-1}{12\eta} \left(\left[h(x) \right]^3 \frac{dp}{dx} - 6\eta \mathcal{U} h(x) \right),$$

and the boundary condition $v(x, h) = 0$, are satisfied exactly when $p(x)$ satisfies the Reynolds equation,

$$(2.9) \quad \frac{d}{dx} \left[\left[h(x) \right]^3 \frac{dp}{dx} \right] = 6\eta \mathcal{U} \frac{dh}{dx}.$$

For the pressure boundary conditions, we consider a mixed Dirichlet-Neumann boundary condition, prescribing the flux \mathcal{Q} and outlet pressure \mathcal{P}_N ,

$$(2.10) \quad \left. \frac{dp}{dx} \right|_{x_0} = \frac{-12\eta \mathcal{Q}}{[h(x_0)]^3} + \frac{6\eta \mathcal{U}}{[h(x_0)]^2}, \quad p(x_N) = \mathcal{P}_N.$$

To translate to a Dirichlet boundary condition, the prescribed flux \mathcal{Q} is exchanged for a prescribed inlet pressure $p(x_0) = \mathcal{P}_0$, corresponding to a prescribed pressure drop $\Delta\mathcal{P} = p(x_N) - p(x_0)$ for the whole domain,

$$(2.11) \quad p(x_N) - p(x_0) = -12\eta \mathcal{Q} \int_{x_0}^{x_N} [h(x)]^{-3} dx + 6\eta \mathcal{U} \int_{x_0}^{x_N} [h(x)]^{-2} dx.$$

In the case that height $h(x)$ is linear, the integrals involving $h(x)$ in (2.11) can be evaluated exactly. Evaluating these integrals is also the key to obtaining an exact solution for the Reynolds equation.

3. The piecewise constant solution. The following method (PWC) for the Reynolds equation considers a piecewise constant approximation of the height function, and utilizes the Schur complement factorization technique (section A) to solve the linear system. In the case that $h(x) > 0$ is constant, the Reynolds equation (2.9) reduces to $\frac{d^2 p}{dx^2} = 0$ and the solution $p(x)$ is linear.

Consider a piecewise constant height $h(x)$ with N components. Let $\{x_k\}_0^N$ demarcate the piecewise constant regions of $h(x)$; denote the widths $\Delta x|_k = x_{k+1} - x_k$. Let $\{h_k\}_0^{N-1}$ denote the constant value of $h(x)$ on (x_k, x_{k+1}) , and let $\{\frac{\Delta p}{\Delta x}|_k\}_0^{N-1}$ denote the constant pressure gradient on (x_k, x_{k+1}) ,

$$(3.1) \quad \left. \frac{\Delta p}{\Delta x} \right|_k = \frac{p_{k+1} - p_k}{x_{k+1} - x_k},$$

where $\{p_k\}_0^N$ are the pressure endpoints, $p_k = p(x_k)$. The flux \mathcal{Q} expressed in (2.8) relates each of the N constant pressure gradients. Eliminating the constant flux gives the relationship,

$$(3.2) \quad h_k^3 \left. \frac{\Delta p}{\Delta x} \right|_k - h_j^3 \left. \frac{\Delta p}{\Delta x} \right|_j + 6\eta \mathcal{U} (h_j - h_k) = 0,$$

for any $j, k \in [0, N - 1]$.

The expressions (3.1) for $k \in [0, N - 1]$ and (3.2) for $j = k + 1, k \in [0, N - 2]$ constitute a size $2N - 1$ linear system $\mathbf{M}\mathbf{x} = \mathbf{b}$ solving for,

$$(3.3) \quad \mathbf{x} = \left[\frac{\Delta p}{\Delta x} \Big|_0, \frac{\Delta p}{\Delta x} \Big|_1, \dots, \frac{\Delta p}{\Delta x} \Big|_{N-1}, p_1, p_2, \dots, p_{N-1} \right]^T.$$

The matrix \mathbf{M} is formulated as a block matrix,

$$(3.4) \quad \mathbf{M} = \left[\begin{array}{c|ccccc} & \mathcal{I} & & & & \\ \hline & & \begin{matrix} 0 & 0 & \dots & 0 \\ \frac{1}{\Delta x_1} & \frac{-1}{\Delta x_1} & \ddots & \vdots \\ 0 & \ddots & \ddots & 0 \\ \vdots & \ddots & \frac{1}{\Delta x_{N-2}} & \frac{-1}{\Delta x_{N-2}} \\ 0 & \dots & 0 & \frac{1}{\Delta x_{N-1}} \end{matrix} \\ \hline & \begin{matrix} -h_0^3 & h_1^3 & 0 & \dots & 0 \\ 0 & -h_1^3 & h_2^3 & \ddots & \vdots \\ \vdots & \ddots & \ddots & \ddots & 0 \\ 0 & \dots & 0 & -h_{N-2}^3 & h_{N-1}^3 \end{matrix} & & & & 0 \end{array} \right],$$

where \mathcal{I} denotes an identity block of size N . The right hand side is given by,

$$(3.5) \quad \mathbf{b} = \left[-12\eta \left(\mathcal{Q}h_0^{-3} - \frac{1}{2}\mathcal{U}h_0^{-2} \right), 0, \dots, 0, \frac{\mathcal{P}_N}{\Delta x_{N-1}}, 6\eta\mathcal{U}(h_1 - h_0), 6\eta\mathcal{U}(h_2 - h_1), \dots, 6\eta\mathcal{U}(h_{N-1} - h_{N-2}) \right]^T.$$

The Schur complement (A.2) is used to evaluate the system $\mathbf{M}\mathbf{x} = \mathbf{b}$. In terms of the block structure (A.1), the inverse for \mathbf{M} is,

$$(3.6) \quad \mathbf{M}^{-1} = \begin{bmatrix} \mathcal{I} + BK^{-1}C & -BK^{-1} \\ -K^{-1}C & K^{-1} \end{bmatrix},$$

where K is the Schur complement of size $N - 1$. In the implementation, one need not compute all entries to the matrix products appearing in the blocks of \mathbf{M}^{-1} , although it is necessary to compute all entries to the dense matrix K^{-1} . At most two entries in the upper block of \mathbf{b} are non-zero, corresponding to the boundary values; on evaluating $\mathbf{M}^{-1}\mathbf{b} = \mathbf{x}$ to solve for $\{p_k\}_{k=1}^{N-1}$, it is only necessary to compute the first and last columns of $-K^{-1}C$. Once the pressure endpoints $\{p_k\}_{k=1}^{N-1}$ are determined, the pressure gradients $\{\frac{\Delta p}{\Delta x}\}_{k=0}^{N-1}$ are easily obtained. In this sense, the solution hinges almost entirely on inverting the Schur complement.

In this case, the Schur complement for \mathbf{M} is simply $K = -CB$, which is a symmetric tri-diagonal matrix, with off-diagonal elements $K_{i,i+1} = K_{i+1,i} = \frac{h_{i+1}^3}{\Delta x_{i+1}}$ and diagonal elements $K_{i,i} = -\left(\frac{h_i^3}{\Delta x_i} + \frac{h_{i+1}^3}{\Delta x_{i+1}}\right)$. An efficient and numerically stable algorithm for the inversion of tri-diagonal matrices is presented in [9], and here we outline the reduced algorithm for the symmetric case.

Let $K_{i,i} = \alpha_i$ for $i \in [0, N-2]$ and $K_{i,i+1} = K_{i+1,i} = \beta_i$ for $i \in [0, N-3]$ denote the diagonal and off-diagonal elements of the Schur complement K . Define the recursive sequence $\{S_k\}_{N-3}^0$ as,

$$(3.7) \quad \begin{cases} S_{N-3} = -\beta_{N-3}/\alpha_{N-2} \\ S_k = -\beta_k/(\alpha_{k+1} + S_{k+1}\beta_{k+1}) \quad k \in [0, N-4] \end{cases}.$$

The diagonal elements of K^{-1} are then obtained recursively as,

$$(3.8) \quad \begin{cases} K_{0,0}^{-1} = 1/(\alpha_0 + \beta_0 S_0) \\ K_{i+1,i+1}^{-1} = (1 - \beta_i K_{i,i}^{-1} S_i)/(\alpha_{i+1} + \beta_{i+1} S_{i+1}) \quad i \in [0, N-3] \\ K_{N-2,N-2}^{-1} = (1 - \beta_{N-3} K_{N-3,N-3}^{-1} S_{N-3})/\alpha_{N-2} \end{cases}$$

and the remaining elements of the symmetric K^{-1} are given by,

$$(3.9) \quad \begin{cases} K_{i,j}^{-1} = K_{i,i}^{-1} \prod_{k=i}^{j-1} S_k \quad i < j \\ K_{i,j}^{-1} = K_{j,i}^{-1} \quad i > j \end{cases}.$$

Through this approach, we gain element-wise access to K^{-1} through two recursive sequences $\{S_k\}_{N-3}^0$ and $\{K_{i,i}^{-1}\}_{0}^{N-2}$. In the implementation, we also precompute the partial product sequence $\{T_k\}_{k=0}^{N-3} = \{\prod_{i=0}^k S_k\}_{k=0}^{N-3}$ so that non-diagonal elements of $K_{i,j}^{-1}$ are evaluated as $K_{i,j}^{-1} = K_{i,i}^{-1} (T_{j-1}/T_{i-1})$. Once K^{-1} is determined, the solution $M^{-1}\mathbf{b} = \mathbf{x}$ can be evaluated. Although K^{-1} can be described in $\mathcal{O}(N)$ time with the two recursive sequences, evaluating $M^{-1}\mathbf{b} = \mathbf{x}$ is done in $\mathcal{O}(N^2)$ time.

4. The piecewise linear solution. The following method (PWL) for the Reynolds equation considers a piecewise linear approximation to the height, and formulates a new linear system that can also be solved using the Schur complement. The PWL method is more general and more efficient than the PWC method. Where the PWC method uses the constant pressure gradients $\frac{\Delta p}{\Delta x}|_k$ as variables in the linear system, the PWL method uses a single variable $\mathcal{C}_Q = -12\eta\mathcal{Q}$ corresponding to the flux, unifying the (now not necessarily constant) pressure gradients $\frac{dp}{dx}|_k$ on each component.

Suppose $h(x)$ defined on $[x_0, x_N]$ is piecewise linear with N components. Let $\{x_k\}_{0}^N$ denote the critical points of $h(x)$ demarcating each piecewise linear region. Let $\{h_{k\pm}\}_{k=0}^N$ denote the endpoints of $h(x)$ on each interval, $h_{k\pm} = \lim_{x \rightarrow x_k^\pm} h(x)$. And let $\{\frac{\Delta h}{\Delta x}|_k\}_{k=0}^{N-1}$ denote the constant gradients of $h(x)$ for each interval,

$$(4.1) \quad \frac{\Delta h}{\Delta x}\Big|_k = \frac{h_{(k+1)-} - h_{k+}}{x_{k+1} - x_k} = \lim_{x \rightarrow x_k^+} \frac{dh}{dx}.$$

The solution to the Reynolds equation for a piecewise linear height is derived from coupling solutions of the form (4.2) on each sub-interval.

For a single interval $[x_k, x_{k+1}]$ on which $h(x)$ is piecewise linear, $p(x)$ satisfies,

$$(4.2) \quad p(x) = \begin{cases} -\left(\frac{1}{2}\mathcal{C}_Q[h(x)]^{-2} + 6\eta\mathcal{U}[h(x)]^{-1}\right)\left[\frac{\Delta h}{\Delta x}\Big|_k\right]^{-1} + \mathcal{C}_{P_k} & \frac{\Delta h}{\Delta x}\Big|_k \neq 0 \\ \left(\mathcal{C}_Q[h(x)]^{-3} + 6\eta\mathcal{U}[h(x)]^{-2}\right)(x - x_k) + \mathcal{C}_{P_k} & \frac{\Delta h}{\Delta x}\Big|_k = 0 \end{cases}.$$

The constant C_Q arises in the first integration of the Reynolds equation and is directly proportional to the flux; comparing with (2.8) gives $\mathcal{C}_Q = -12\eta\mathcal{Q}$. The constant C_{P_k} arises in the second integration of the Reynolds equation and relates to the fixed endpoint pressure. For $h(x)$ with N piecewise linear components, we couple solutions of the form (4.2). The fixed outlet pressure $p(x_N) = \mathcal{P}_N$ determines $\mathcal{C}_{P_{N-1}}$,

$$(4.3) \quad \mathcal{C}_{P_{N-1}} = \begin{cases} \mathcal{P}_N + \mathcal{C}_Q \frac{1}{2} \frac{\Delta h}{\Delta x} \Big|_{N-1}^{-1} h_{N-}^{-2} + 6\eta\mathcal{U} \frac{\Delta h}{\Delta x} \Big|_{N-1}^{-1} h_{N-}^{-1} \frac{\Delta h}{\Delta x} \Big|_{N-1} \neq 0 \\ \mathcal{P}_N - \mathcal{C}_Q h_{N-}^{-3} \Delta x \Big|_{N-1} - 6\eta\mathcal{U} h_{N-}^{-2} \Delta x \Big|_{N-1} \frac{\Delta h}{\Delta x} \Big|_{N-1} = 0 \end{cases}.$$

To solve for $\{\mathcal{C}_{P_k}\}_{k=0}^{N-2}$, we assume a continuous pressure $p(x)$ and set the left and right limits equal at each x_k ,

$$(4.4) \quad \lim_{x \rightarrow x_k^-} p(x) = \begin{cases} -\frac{\Delta h}{\Delta x} \Big|_{k-1}^{-1} \left(\frac{1}{2} \mathcal{C}_Q h_{k-}^{-2} + 6\eta\mathcal{U} h_{k-}^{-1} \right) + \mathcal{C}_{P_{k-1}} \frac{\Delta h}{\Delta x} \Big|_{k-1} \neq 0 \\ \Delta x \Big|_{k-1} \left(\mathcal{C}_Q h_{k-}^{-3} + 6\eta\mathcal{U} h_{k-}^{-2} \right) + \mathcal{C}_{P_{k-1}} \frac{\Delta h}{\Delta x} \Big|_{k-1} = 0 \end{cases},$$

$$(4.5) \quad \lim_{x \rightarrow x_k^+} p(x) = \begin{cases} -\frac{\Delta h}{\Delta x} \Big|_k^{-1} \left(\frac{1}{2} \mathcal{C}_Q h_{k+}^{-2} + 6\eta\mathcal{U} h_{k+}^{-1} \right) + \mathcal{C}_{P_k} \frac{\Delta h}{\Delta x} \Big|_k \neq 0 \\ \mathcal{C}_{P_k} \frac{\Delta h}{\Delta x} \Big|_k = 0 \end{cases}.$$

Hence for each $0 < k < N$, the integration constants C_{P_k} , $C_{P_{k-1}}$ and C_Q satisfy,

$$(4.6) \quad \begin{cases} \mathcal{C}_{P_k} - \mathcal{C}_{P_{k-1}} - \mathcal{C}_Q \left(\frac{1}{2} h_{k+}^{-2} \frac{\Delta h}{\Delta x} \Big|_k^{-1} - \frac{1}{2} h_{k-}^{-2} \frac{\Delta h}{\Delta x} \Big|_{k-1}^{-1} \right) \\ = 6\eta\mathcal{U} \left(h_{k+}^{-1} \frac{\Delta h}{\Delta x} \Big|_k^{-1} - h_{k-}^{-1} \frac{\Delta h}{\Delta x} \Big|_{k-1}^{-1} \right) \quad \frac{\Delta h}{\Delta x} \Big|_k \neq 0, \frac{\Delta h}{\Delta x} \Big|_{k-1} \neq 0 \\ \mathcal{C}_{P_k} - \mathcal{C}_{P_{k-1}} - \mathcal{C}_Q \left(\frac{1}{2} h_{k+}^{-2} \frac{\Delta h}{\Delta x} \Big|_k^{-1} + h_{k-}^{-3} \Delta x \Big|_{k-1} \right) \\ = 6\eta\mathcal{U} \left(h_{k+}^{-1} \frac{\Delta h}{\Delta x} \Big|_k^{-1} + h_{k-}^{-2} \Delta x \Big|_{k-1} \right) \quad \frac{\Delta h}{\Delta x} \Big|_k \neq 0, \frac{\Delta h}{\Delta x} \Big|_{k-1} = 0 \\ \mathcal{C}_{P_k} - \mathcal{C}_{P_{k-1}} + \mathcal{C}_Q \frac{1}{2} h_{k-}^{-2} \frac{\Delta h}{\Delta x} \Big|_{k-1}^{-1} \\ = -6\eta\mathcal{U} h_{k-}^{-1} \frac{\Delta h}{\Delta x} \Big|_{k-1}^{-1} \quad \frac{\Delta h}{\Delta x} \Big|_k = 0, \frac{\Delta h}{\Delta x} \Big|_{k-1} \neq 0 \\ \mathcal{C}_{P_k} - \mathcal{C}_{P_{k-1}} - \mathcal{C}_Q h_{k-}^{-3} \Delta x \Big|_{k-1} \\ = 6\eta\mathcal{U} h_{k-}^{-2} \Delta x \Big|_{k-1} \quad \frac{\Delta h}{\Delta x} \Big|_k = 0, \frac{\Delta h}{\Delta x} \Big|_{k-1} = 0 \end{cases}$$

All together, C_Q and $\{\mathcal{C}_{P_k}\}_{k=0}^{N-1}$ constitute a size $N+1$ linear system of equations $\mathbf{M}\mathbf{x} = \mathbf{b}$ where $\mathbf{x} = [\mathcal{C}_Q, \mathcal{C}_{P_0}, \dots, \mathcal{C}_{P_{N-1}}]^T$. Corresponding to (4.6), the matrix \mathbf{M} stores the coefficients on C_Q , \mathcal{C}_{P_k} , $\mathcal{C}_{P_{k-1}}$, and the right hand side vector \mathbf{b} holds constant terms. For example, if $\frac{\Delta h}{\Delta x} \Big|_k \neq 0$ for all k ,

$$(4.7) \quad \mathbf{M} = \begin{bmatrix} 1 & 0 & \cdots & 0 \\ -\frac{1}{2} \left(h_{1+}^{-2} \frac{\Delta h}{\Delta x} \Big|_1^{-1} - h_{1-}^{-2} \frac{\Delta h}{\Delta x} \Big|_0^{-1} \right) & -1 & 1 & 0 & \cdots & 0 \\ \vdots & \ddots & \ddots & \ddots & & \vdots \\ -\frac{1}{2} \left(h_{k+}^{-2} \frac{\Delta h}{\Delta x} \Big|_k^{-1} - h_{k-}^{-2} \frac{\Delta h}{\Delta x} \Big|_{k-1}^{-1} \right) & 0 & -1 & 1 & 0 & \cdots \\ \vdots & \vdots & \ddots & \ddots & \ddots & \vdots \\ -\frac{1}{2} \left(h_{N-1+}^{-2} \frac{\Delta h}{\Delta x} \Big|_{N-1}^{-1} - h_{N-1-}^{-2} \frac{\Delta h}{\Delta x} \Big|_{N-2}^{-1} \right) & 0 & \cdots & 0 & -1 & 1 \\ \frac{1}{2} h_N^{-2} \frac{\Delta h}{\Delta x} \Big|_{N-1}^{-1} & 0 & \cdots & 0 & -1 & 0 \end{bmatrix},$$

and,

$$(4.8) \quad \mathbf{b} = \left[-12\eta\mathcal{Q}, 6\eta\mathcal{U}\left(h_{1^+}^{-1}\frac{\Delta h}{\Delta x}\Big|_1^{-1} - h_{1^-}^{-1}\frac{\Delta h}{\Delta x}\Big|_0^{-1}\right), \dots, 6\eta\mathcal{U}\left(h_{k^+}^{-1}\frac{\Delta h}{\Delta x}\Big|_k^{-1} - h_{k^-}^{-1}\frac{\Delta h}{\Delta x}\Big|_{k-1}^{-1}\right), \dots, -6\eta\mathcal{U}h_N^{-1}\frac{\Delta h}{\Delta x}\Big|_{N-1}^{-1} - \mathcal{P}_N \right]^T.$$

The matrix \mathbf{M} has a block form; in view of the structure (A.1), $A = 1$, $B = 0$, C is the vector of C_Q coefficients from (4.6), and D is a bi-diagonal matrix corresponding to the C_{P_k} and $C_{P_{k-1}}$ coefficients from (4.6). Since $B = 0$, the Schur complement (A.2) is simply $K = D$, and the inverse of \mathbf{M} is,

$$(4.9) \quad \mathbf{M}^{-1} = \begin{bmatrix} 1 & 0 \\ -D^{-1}C & D^{-1} \end{bmatrix}.$$

The matrix $K^{-1} = D^{-1}$ is upper triangular with all -1 entries. The matrix vector product $-D^{-1}C$ is then the reversed partial sum of entries in C . Likewise, when evaluating $\mathbf{M}^{-1}\mathbf{b}$, the lower block of \mathbf{b} is multiplied by D^{-1} , resulting in the negative reversed partial sum of these entries in \mathbf{b} . In this case, solving with the Schur complement is equivalent to reducing the identity row in \mathbf{M} : solving C_Q and moving the block C to the right hand side. After solving for \mathbf{x} comprising C_Q and $\{C_{P_k}\}_{k=0}^{N-1}$, the pressure $p(x)$ on each region $\{[x_k, x_{k+1}]\}_{k=0}^{N-1}$ is obtained according to (4.2).

The PWL method for the Reynolds equation is more efficient than the less general PWC method. In the PWC method, we independently compute each entry to K^{-1} when we evaluate $\mathbf{M}^{-1}\mathbf{b} = \mathbf{x}$, leading to an $\mathcal{O}(N^2)$ time algorithm. In the PWL method, K^{-1} is constant and upper triangular, so $\mathbf{M}^{-1}\mathbf{b} = \mathbf{x}$ can be evaluated through computing two partial sums in an $\mathcal{O}(N)$ time algorithm.

5. Examples. We now consider a variety of textured slider examples to evaluate the PWL and PWC methods for the Reynolds equation. We compare the PWC and PWL solutions with a finite difference (FD) solution for the Reynolds equation (section B), and with a finite difference solution to the Stokes equation (section C). We examine both piecewise linear and non-linear height functions: the backward facing step, the wedge slider, the logistic step, and the sinusoidal slider. For the latter two examples, the PWC and PWL methods consider approximations to the non-linear height. These examples feature surface discontinuities and large surface gradients to showcase the differences in the pressure and velocity solutions from the Reynolds and the Stokes equations.

5.1. Piecewise constant height. The backward facing step is a classical example in lubrication theory; this piecewise constant height features a single discontinuity,

$$(5.1) \quad h(x) = \begin{cases} H_{\text{in}} & 0 \leq x < l \\ H_{\text{out}} & l \leq x \leq L \end{cases},$$

where $H_{\text{in}} > H_{\text{out}}$. Both the PWC and the PWL methods for the Reynolds equation give the exact solution to the backward facing step. Note that the FD method for the Reynolds equation converges to this exact solution at order only $\mathcal{O}(\Delta x)$; despite using a second-order accurate differences, the jump discontinuity in $h(x)$ prevents $\mathcal{O}(\Delta x^2)$ convergence.

The pressure and velocity solutions to the backward facing step with the Reynolds and the Stokes equations are shown in Figure 5.1 for $H_{\text{in}} = 2$, $H_{\text{out}} = 1$, $l = 8$, $L = 16$, and with the boundary conditions $\mathcal{Q} = 1$, $\mathcal{P}_N = 0$, $\mathcal{U} = 0$. The solution to the Stokes equation displays significant cross film pressure variation in the vicinity of the step that the Reynolds equation does not capture. The solution to the Reynolds equation underestimates the total pressure drop ΔP . Moreover, velocity for the Stokes equation depicts corner flow recirculation, whereas the velocity solution from the Reynolds equation is discontinuous at the step due to the surface discontinuity.

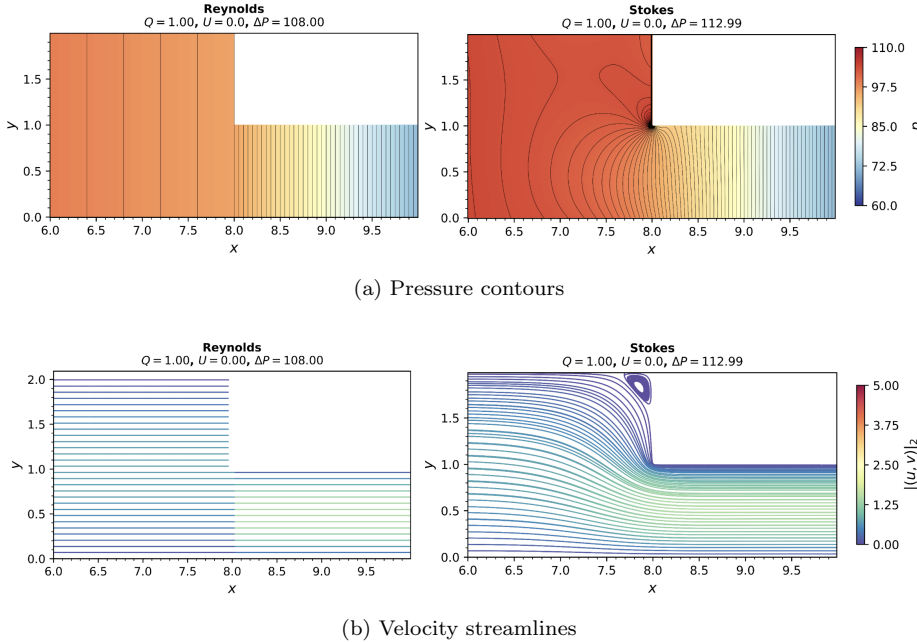


FIG. 5.1. The pressure and velocity solutions for the backward facing step with the Reynolds equation (left) and the Stokes equation (right). The solution to the Reynolds equation underestimates the pressure drop ΔP , and does not capture corner flow recirculation.

5.2. Piecewise linear height. Next we consider the wedge slider; the continuous piecewise linear height is given by,

$$(5.2) \quad h(x) = \begin{cases} H_{\text{in}} & 0 \leq x < l_{\text{in}} \\ H_{\text{in}} + \frac{H_{\text{out}} - H_{\text{in}}}{l_{\text{wedge}}}(x - l_{\text{in}}) & l_{\text{in}} \leq x < l_{\text{in}} + l_{\text{wedge}}, \\ H_{\text{out}} & l_{\text{in}} + l_{\text{wedge}} \leq x \leq L \end{cases}$$

where $L = l_{\text{in}} + l_{\text{out}} + l_{\text{wedge}}$, $H_{\text{in}} > H_{\text{out}}$ and $l_{\text{wedge}} > 0$. Here, the PWL method gives the exact solution to the Reynolds equation, and both the PWC method and the FD method converge to the exact solution at order $\mathcal{O}(\Delta x^2)$.

The pressure and velocity solutions to the wedge slider for the Reynolds and the Stokes equations are shown in Figure 5.2 for $H_{\text{in}} = 2$, $H_{\text{out}} = 1$, $l_{\text{in}} = l_{\text{out}} = 7$, $l_{\text{wedge}} = 2$, $L = 16$, and with the boundary conditions $\mathcal{Q} = 1$, $\mathcal{P}_N = 0$, $\mathcal{U} = 0$. For this case of a moderately sloped wedge, the Reynolds equation is a fair approximation to the Stokes equation. However, the vertical velocity v corresponding to the Reynolds equation is not x -continuous at the discontinuities in the surface gradient, and the

discontinuity in v is more pronounced when the height is larger. As the slope of the wedge increases, the wedge slider limits to the backward facing step, and the solution of the Reynolds equation diverges from that of the Stokes equation.

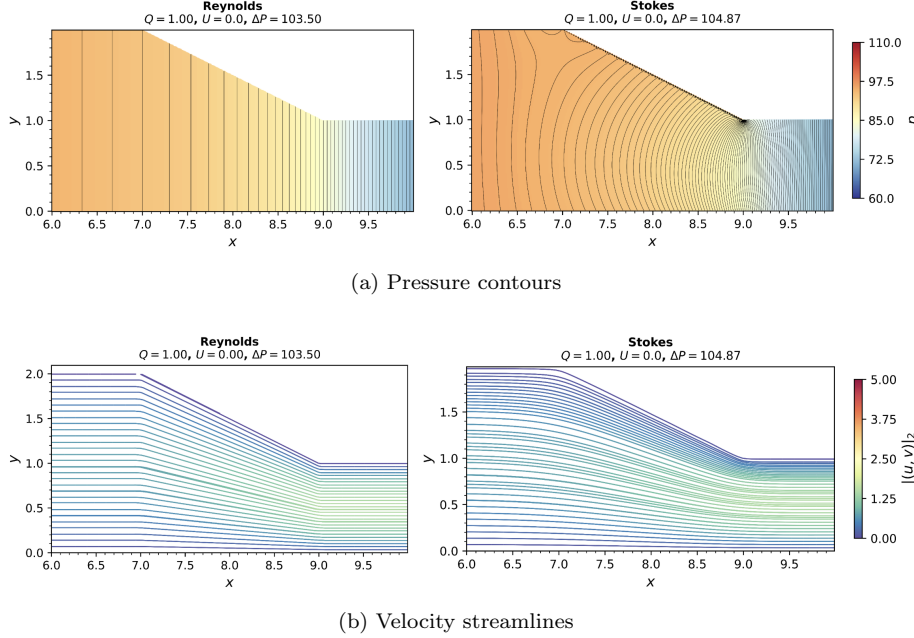


FIG. 5.2. The pressure and velocity solutions for the wedge slider with the Reynolds equation (left) and the Stokes equation (right). The solutions to the Reynolds and the Stokes equations are similar in the case of a moderately sloped wedge.

5.3. Piecewise smooth heights. Next we consider two piecewise smooth geometries: a logistic step and a sinusoidal slider. For these examples, the piecewise constant, piecewise linear and finite difference methods for the Reynolds equation are all numerical approximations. Convergence testing against an exact solution for the sinusoidal slider is presented in section D.

To utilize the PWL and PWC solvers for heights which are not piecewise constant or piecewise linear, we consider suitable approximations to the height function. Where the FD method uses $N + 1$ grid points $\{x_i\}_{i=0}^N$ and discretizes the height as $\{h_i\}_{i=0}^N$, the PWC method considers N intervals $\{[x_i, x_{i+1}]\}_{i=0}^{N-1}$ and constant heights $\{\frac{1}{2}(h_{i+1} + h_i)\}_{i=0}^{N-1}$ for each interval. Likewise, the PWL method considers N intervals $\{[x_i, x_{i+1}]\}_{i=0}^{N-1}$ with the same height discretization $\{h_i\}_{i=0}^N$ as the FD method, corresponding to N constant height gradients $\{\frac{\Delta h}{\Delta x}\}_{i=0}^{N-1}$ for each interval.

5.3.1. The logistic step. The logistic step is a smooth analogue to the backward facing step and wedge slider. The height is given by,

$$(5.3) \quad h(x) = H_{\text{in}} + \frac{H_{\text{out}} - H_{\text{in}}}{1 + e^{\lambda(L/2-x)}},$$

where $H_{\text{in}} \geq H_{\text{out}} > 0$ are the inlet and outlet heights, and $\lambda > 0$ corresponds to the surface gradient, $\max |\frac{dh}{dx}| = \lambda(H_{\text{in}} - H_{\text{out}})/4$ at the midpoint $x = L/2$.

The pressure and velocity solutions to the logistic step for the Reynolds and the Stokes equations are shown in Figure 5.3 for $H_{\text{in}} = 2$, $H_{\text{out}} = 1$, $\lambda = 32$, $L = 16$, and with the boundary conditions $Q = 1$, $\mathcal{P}_N = 0$, $\mathcal{U} = 0$. As with the wedge slider and the backward facing step, the solutions from the Reynolds and the Stokes equations are dissimilar in the presence of large surface gradients. The pressure for the Stokes equation has significant cross film pressure variation $\frac{\partial p}{\partial y}$ in the vicinity of the large surface gradient, whereas the pressure for the Reynolds equation is necessarily one dimensional. At this steep of slope, the velocity for the Stokes equation depicts flow recirculation similar to the backward facing step in Figure 5.1. The velocity for the Reynolds equation does not have flow recirculation, and the velocity magnitude is overestimated in the vicinity of the large surface gradient.

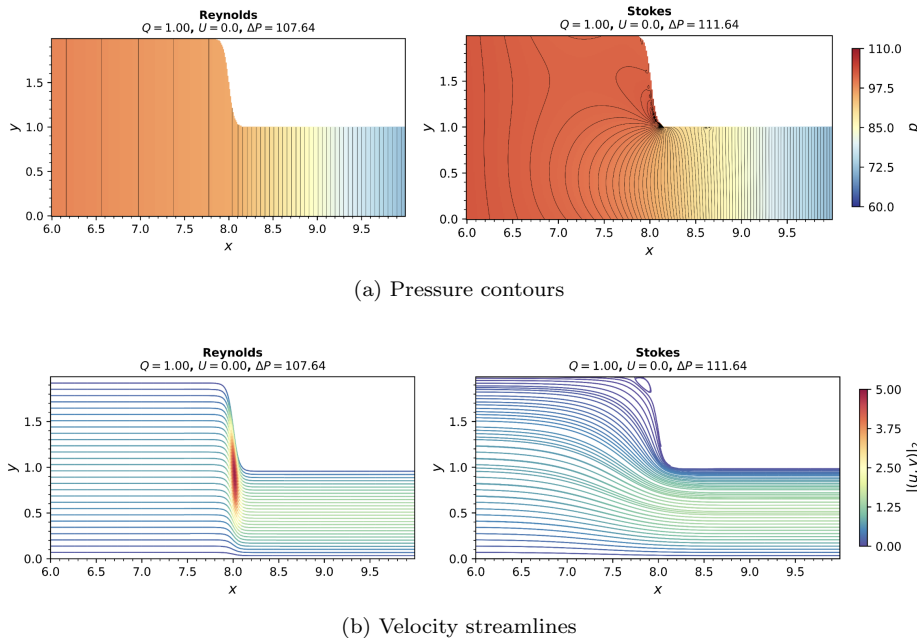


FIG. 5.3. The pressure and velocity solutions for the logistic step with the Reynolds equation (left) and the Stokes equation (right). As with the backward facing step, the Reynolds equation underestimates the pressure drop ΔP , and does not capture cross film pressure variation or corner flow recirculation as seen with the Stokes equation.

5.3.2. The sinusoidal slider. Compared with the previous examples which are all variations on a step texture, the sinusoidal slider exhibits a cavity texture. The height is,

$$(5.4) \quad h(x) = \begin{cases} H_0(1 + \delta) & l < |x| < L, \ k \text{ even} \\ H_0(1 - \delta) & l < |x| < L, \ k \text{ odd} \\ H_0(1 + \delta \cos(x\pi k/l)) & |x| < l \end{cases},$$

where k is the integer wave number on length $2l$, H_0 is the equilibrium height, $\delta \in [0, 1]$ gives the amplitude δH_0 , and $2L$ is the total length. The regions of constant height at the inlet and outlet are aligned with the extrema of the sinusoid, keeping the height gradient continuous. When k is odd, k is the number of positive textures and

$\min h(x) = H_0(1 - \delta)$ is the inlet and outlet height. When k is even, k is the number of negative textures and $\max h(x) = H_0(1 + \delta)$ is the inlet and outlet height.

The pressure and velocity solutions to the sinusoidal slider for the Reynolds and the Stokes equations are shown in Figure 5.4 for $H_0 = 1$, $\delta = 1/2$, $k = 2$, $l = 1$, $L = 8$, and with the boundary conditions $Q = 1$, $\mathcal{P}_N = 0$, $\mathcal{U} = 0$. The velocity for the Stokes equation depicts flow recirculation in the region of positive texturing that the Reynolds equation does not capture. The velocity magnitude for the Stokes equation is largest at the valleys of the sinusoid, whereas for the Reynolds equation, the velocity magnitude is largest either side of these valleys where the surface gradient is large. In general, for regions where the surface gradient is large relative to the height, and the solution to Stokes equation has significant cross film pressure variation $\frac{\partial p}{\partial y}$, the Reynolds equation tends to overestimate the velocity magnitude.

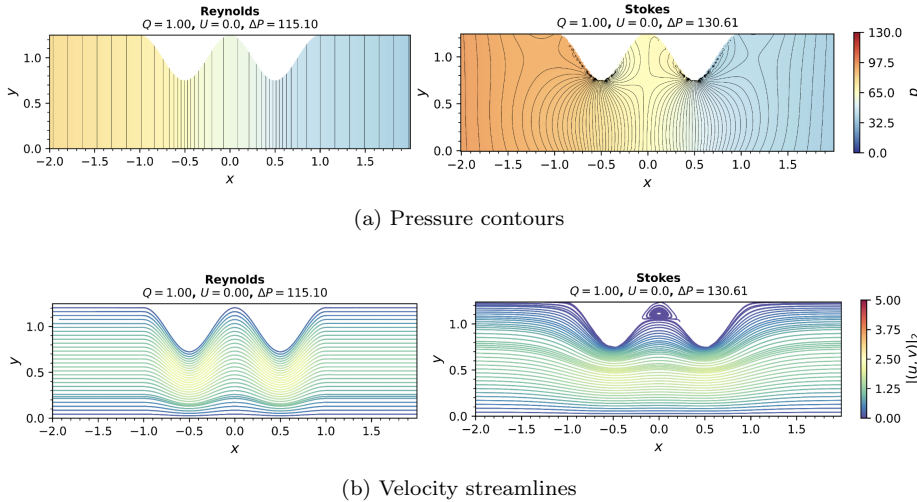


FIG. 5.4. The pressure and velocity solutions for the sinusoidal slider with the Reynolds equation (left) and the Stokes equation (right). The Reynolds equation overestimates the velocity magnitude when the surface gradient is large and the height is small.

6. Timing. When the height is piecewise constant or piecewise linear, the PWC and PWL methods give the exact solution to the Reynolds equation and are certainly faster than the FD solution. The PWC and PWL methods scale with the number of piecewise components, whereas the FD method requires a fine grid resolution to capture steep slopes and surface discontinuities.

When the height is non-linear, the PWC, PWL and FD methods all approximate the solution on a grid. Recall, where the FD method uses $N + 1$ grid points, the PWC and PWL methods use N piecewise components; the grid spacing in both cases is $\Delta x = 1/N$. Figure 6.1 shows the computational run times for the FD, PWC, and PWL methods with the logistic step example. For a non-linear height, the PWL method is significantly faster than both the PWC and FD methods. The FD method is evaluated with `numpy.linalg.solve`, which is an LU method with partial pivoting, having $\mathcal{O}(N^3)$ time complexity. In the PWC method, a nested loop is used to compute each element of the Schur complement inverse $K_{i,j}^{-1}$ when we evaluate $M^{-1}\mathbf{b}$, leading to $\mathcal{O}(N^2)$ complexity. In the PWL method, the upper triangular Schur complement is simple invert and $M^{-1}\mathbf{b}$ can be evaluated in a single loop, corresponding to $\mathcal{O}(N)$

complexity. These time complexities are confirmed by the timing results in [Figure 6.1](#).

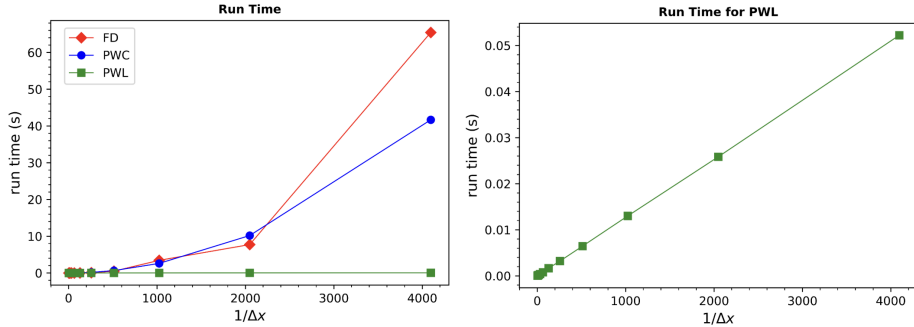


FIG. 6.1. The PWL method is linear time and faster than the PWC method (quadratic time) and the FD method (cubic time).

7. Conclusions. We presented the piecewise constant (PWC) and piecewise linear (PWL) methods for the Reynolds equation and compared with the finite difference (FD) method. The PWC and PWL methods take advantage of the exact solution to the Reynolds equation when the height is piecewise linear, and couple the exact solution for each piecewise component using the assumption of constant flux and continuous pressure. The PWC and PWL methods seamlessly handle discontinuities in the surface and retain their second order accuracy, compared with the FD method which has reduced order of accuracy in the case of surface discontinuities. The PWL method takes advantage of the constant flux to model the pressure gradients on each piecewise component, whereas the PWC method treats each constant pressure gradient as a solution variable. As a result, the PWL method is the most computationally efficient, running with linear time complexity.

We then compared the solutions of pressure and velocity for the Reynolds and the Stokes equations. The pressure from the Stokes equation exhibits significant cross film pressure variation in the presence of large surface gradients or surface discontinuities. The pressure from the Reynolds equation has no cross film pressure variation, leading to an underestimation of the overall pressure drop in the case of large surface gradients or discontinuous surface discontinuities compared. For the backward facing step, and in the logistic step and sinusoidal slider with large slopes, the velocity from the Stokes equation depicts corner flow recirculation. The velocity from the Reynolds equation does not correctly model flow recirculation compared with the Stokes equations, and the magnitude of velocity from the Reynolds equation is overestimated when large surface gradients occur alongside small heights. Moreover, the velocities from the Reynolds equation are discontinuous at discontinuities in the surface, and the vertical velocity is also discontinuous at discontinuities in the surface gradient. Ultimately, the Reynolds equation is best suited for the case of continuous and slowly varying surface geometries.

Acknowledgments. This work was supported by National Science Foundation (NSF) grant DMS-2512565 to TGF. We also acknowledge use of the Brandeis High Performance Computing Cluster (HPCC) which is partially supported by the NSF through DMR-MRSEC 2011846 and OAC-1920147.

Appendix A. The Schur complement. The Schur complement is a linear algebra technique utilized in the factorization and inversion of block matrices. The theory is presented in [7] and summarized here. Given a block matrix,

$$(A.1) \quad M = \begin{bmatrix} A & B \\ C & D \end{bmatrix}$$

where A is invertible, the Schur complement of M is given by

$$(A.2) \quad K = D - CA^{-1}B.$$

Through Gaussian elimination, the Schur complement K gives a block LDU decomposition for M ,

$$(A.3) \quad M = \begin{bmatrix} \mathcal{I} & 0 \\ CA^{-1} & \mathcal{I} \end{bmatrix} \begin{bmatrix} A & 0 \\ 0 & K \end{bmatrix} \begin{bmatrix} \mathcal{I} & A^{-1}B \\ 0 & \mathcal{I} \end{bmatrix},$$

and reduces the problem of finding M^{-1} to finding K^{-1} and A^{-1} . Following the process of forward and backward substitution from the block LDU decomposition for M , the general form of M^{-1} is derived,

$$(A.4) \quad M^{-1} = \begin{bmatrix} A^{-1} + A^{-1}BK^{-1}CA^{-1} & -A^{-1}BK^{-1} \\ -K^{-1}CA^{-1} & K^{-1} \end{bmatrix}.$$

Appendix B. Finite difference method for the Reynolds equation.

First, we present a finite difference solution to the Reynolds equation. Define the uniform discretisation of the domain $[x_0, x_L]$,

$$(B.1) \quad \{x_i\}_{i=0}^N, \quad x_i = x_0 + i\Delta x, \quad \Delta x = \frac{1}{N}|x_L - x_0|.$$

A second-order accurate difference approximation for the Reynolds equation (2.9) is,

$$(B.2) \quad \frac{1}{2\Delta x^2} \left((h_{i+1}^3 + h_i^3)p_{i+1} - (h_{i+1}^3 + 2h_i^3 + h_{i-1}^3)p_i + (h_i^3 + h_{i-1}^3)p_{i-1} \right) = \frac{6\eta\mathcal{U}}{2\Delta x} (h_{i+1} - h_{i-1}),$$

where $h_i = h(x_i)$ and $p_i = p(x_i)$. The form (B.2) is obtained by approximating the outer derivative on the left-hand-side of (2.9) on half grid points,

$$\left[\frac{d}{dx} \left[[h(x)]^3 \frac{dp}{dx} \right] \right]_i = \frac{\left[[h(x)]^3 \frac{dp}{dx} \right]_{i+1/2} - \left[[h(x)]^3 \frac{dp}{dx} \right]_{i-1/2}}{\Delta x},$$

and using an average to approximate the height function at the half grid points,

$$\left[[h(x)]^3 \frac{dp}{dx} \right]_{i\pm 1/2} = \frac{\pm (h_{i\pm 1}^3 + h_i^3)(p_{i\pm 1} - p_i)}{2\Delta x}.$$

The flux \mathcal{Q} boundary condition is incorporated through a right-sided difference,

$$\left. \frac{dp}{dx} \right|_0 = \frac{3p_0 - 4p_1 + p_2}{2\Delta x} = \frac{-12\eta\mathcal{Q}}{h_0^3} + \frac{6\eta\mathcal{U}}{h_0^2}.$$

The prescribed outlet pressure is simply applied as $p_N = \mathcal{P}_N$.

The equation (B.2) for $0 < i < N$ and the two boundary conditions associated with $i = 0$ and $i = N$ characterize a size $N + 1$ linear system solving the Reynolds equation for $\{p_k\}_0^N$. We utilize `numpy.linalg.solve` to evaluate this linear system.

Appendix C. Finite difference method for the Stokes equation. The biharmonic formulation of the incompressible Navier-Stokes equations is an effective method of solution for low Reynolds number flows [8, 11, 13, 3]. Through introduction of the stream function $\psi(x, y)$ satisfying,

$$(C.1) \quad u = \frac{\partial \psi}{\partial y} \quad v = -\frac{\partial \psi}{\partial x},$$

the Navier-Stokes equations,

$$(C.2) \quad \frac{\partial p}{\partial x} = \nu \left(\frac{\partial^2 u}{\partial x^2} + \frac{\partial^2 u}{\partial y^2} \right) - \left(u \frac{\partial u}{\partial x} + v \frac{\partial u}{\partial y} \right),$$

$$(C.3) \quad \frac{\partial p}{\partial y} = \nu \left(\frac{\partial^2 v}{\partial x^2} + \frac{\partial^2 v}{\partial y^2} \right) - \left(u \frac{\partial v}{\partial x} + v \frac{\partial v}{\partial y} \right),$$

are expressed as,

$$(C.4) \quad \nabla^4 \psi = \text{Re} (v \nabla^2 u - u \nabla^2 v).$$

When $\text{Re} = 0$, the velocity-stream formulation (C.4) reduces to the biharmonic Stokes equation $\nabla^4 \psi = 0$.

To compare the solution to the Stokes equation with the one dimensional lubrication theory solution, we assume the inlet and outlet flow profiles correspond to a fully developed laminar flow with flux \mathcal{Q} , and restrict to examples with a zero height gradient in the vicinity of the inlet and outlet. The surface boundary conditions for velocity are (2.4) and (2.5), and the pressure satisfies (2.10). The inlet and outlet velocity profiles are,

$$(C.5) \quad u(x_0, y) = u_{\text{Re}}(x_0, y) \quad \frac{\partial u}{\partial x} \Big|_{x_L, y} = 0,$$

$$(C.6) \quad v(x_0, y) = 0 \quad v(x_L, y) = 0,$$

where $u_{\text{Re}}(x, y)$ is the Reynolds equation velocity (2.6) expressed in terms of \mathcal{Q} from (2.8). The corresponding boundary conditions for the stream function ψ are,

$$(C.7) \quad \psi(x_0, y) = \int_0^y u_{\text{Re}}(x, \hat{y}) d\hat{y} \quad \frac{\partial \psi}{\partial x} \Big|_{x_L, y} = 0,$$

$$(C.8) \quad \psi(x, 0) = 0 \quad \psi(x, h(x)) = \mathcal{Q},$$

where,

$$(C.9) \quad \int_0^y u_{\text{Re}}(x, \hat{y}) d\hat{y} = \frac{\mathcal{Q} y^2}{[h(x)]^3} (3h(x) - 2y) + \frac{\mathcal{U} y}{[h(x)]^2} (h(x) - y)^2.$$

The solution ψ , u , v to the biharmonic Navier-Stokes equations (C.1) and (C.4) is determined through an iterative second-order accurate finite difference method as given in [3, 8].

Once the stream and velocity have sufficiently converged, the pressure partial derivatives are determined using a centered second-order accurate finite difference discretisation of the Navier-Stokes equations (C.2) and (C.3). For (C.2),

$$(C.10) \quad \frac{\partial p}{\partial x} \Big|_{i,j} = \frac{\nu}{\Delta x^2} \left(u_{i-1,j} + u_{i+1,j} - 4u_{i,j} + u_{i,j-1} + u_{i,j+1} \right) - \frac{1}{2\Delta x} \left(u_{i,j}(u_{i+1,j} - u_{i-1,j}) + v_{i,j}(u_{i,j+1} - u_{i,j-1}) \right),$$

and $\frac{\partial p}{\partial y}$ as in (C.3) is similar. The pressure $p(x, y)$ is then determined numerically by a path integral from the outlet.

Appendix D. Convergence. We test the grid convergence of the FD, PWL and PWC methods with a sinusoidal slider for which the Reynolds equation has an exact solution [15]. The height is given by,

$$(D.1) \quad h(x) = H_0(1 + \delta \cos(\alpha x))$$

where $H_0 > 0$ is the equilibrium height, $H_0(1 + \delta)$ is the maximum height ($\delta > 0$), and $\alpha \neq 0$ is the period. The exact pressure for the Reynolds equation assumes a fixed pressure boundary condition $\Delta P = 0$. The pressure is given by,

$$(D.2) \quad p(x) = \frac{-6\eta\mathcal{U}\delta(H_0 + h) \sin(\alpha x)}{\alpha H_0^3(2 + \delta^2)(1 + \delta \cos(\alpha x))^2}$$

From (2.8) or (2.11), the flux \mathcal{Q} corresponding to $\Delta P = 0$ is $\mathcal{Q} = \frac{\mathcal{U}\eta H_0(1 - \delta^2)}{2 + \delta^2}$.

The convergence tests for the sinusoidal slider confirm that the all three methods for the Reynolds equation – the finite difference method and both piecewise constant and piecewise linear Schur complement methods – converge to the exact solution at $\mathcal{O}(\Delta x^2)$ in absolute error for ΔP and in l_1 , l_2 , and l_∞ norm error for $p(x)$. Figure D.1 shows the rate of convergence in l_2 norm error for $p(x)$ for the sinusoidal slider with $H_0 = 1$, $\alpha = 2\pi$, $\delta = 1/2$, $\mathcal{U} = 3$, $\mathcal{Q} = 1$.

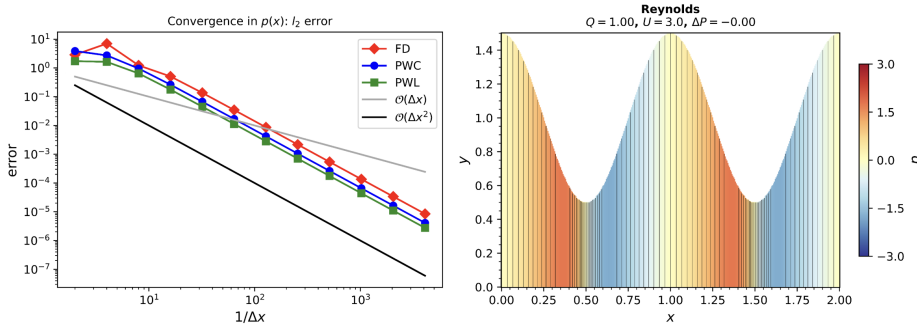


FIG. D.1. Convergence of solutions to the Reynolds equation for the given sinusoidal slider.

REFERENCES

[1] B. F. ARMALY, F. DURST, J. C. F. PEREIRA, AND B. SCHÖNUNG, *Experimental and theoretical investigation of backward-facing step flow*, Journal of Fluid Mechanics, 127 (1983), p. 473, <https://doi.org/10.1017/S0022112083002839>.

- [2] G. BISWAS, M. BREUER, AND F. DURST, *Backward-Facing Step Flows for Various Expansion Ratios at Low and Moderate Reynolds Numbers*, Journal of Fluids Engineering-Transactions of the Asme, 126 (2004), pp. 362–374, <https://doi.org/10.1115/1.1760532>.
- [3] S. BISWAS AND J. KALITA, *HOC simulation of Moffatt eddies and its flow topology in the triangular cavity flow*, Oct. 2017, <https://doi.org/10.48550/arXiv.1710.06251>.
- [4] R. S. BROWN, H. W. STOCKMAN, AND S. J. REEVES, *Applicability of the Reynolds equation for modeling fluid flow between rough surfaces*, Geophysical Research Letters, 22 (1995), pp. 2537–2540, <https://doi.org/10.1029/95GL02666>.
- [5] M. DOBRICA AND M. FILLON, *About the validity of Reynolds equation and inertia effects in textured sliders of infinite width*, Proceedings of the Institution of Mechanical Engineers, Part J: Journal of Engineering Tribology, 223 (2009), pp. 69–78, <https://doi.org/10.1243/13506501JET433>.
- [6] M. B. DOBRICA AND M. FILLON, *Reynolds' Model Suitability in Simulating Rayleigh Step Bearing Thermohydrodynamic Problems*, Tribology Transactions, 48 (2005), pp. 522–530, <https://doi.org/10.1080/05698190500385088>.
- [7] J. GALLIER, *Geometric Methods and Applications: For Computer Science and Engineering*, vol. 38 of Texts in Applied Mathematics, Springer New York, New York, NY, 2011, <https://doi.org/10.1007/978-1-4419-9961-0>.
- [8] M. GUPTA AND J. KALITA, *A new paradigm for solving Navier–Stokes equations: streamfunction–velocity formulation*, Journal of Computational Physics, 207 (2005), pp. 52–68, <https://doi.org/10.1016/j.jcp.2005.01.002>.
- [9] J. JAIN, H. LI, S. CAULEY, C.-K. KOH, AND V. BALAKRISHNAN, *Numerically Stable Algorithms for Inversion of Block Tridiagonal and Banded Matrices*, ECE Technical Reports, (2007), <http://docs.lib.psu.edu/ecetr/357>.
- [10] L. G. LEAL, *Advanced Transport Phenomena*, Cambridge University Press, 2007.
- [11] F. MARNER, P. GASKELL, AND M. SCHOLLE, *On a potential-velocity formulation of Navier–Stokes equations*, Physical Mesomechanics, 17 (2014), pp. 124–130, <https://doi.org/10.1134/S1029959914040110>.
- [12] R. RAHMANI, I. MIRZAEE, A. SHIRVANI, AND H. SHIRVANI, *An analytical approach for analysis and optimisation of slider bearings with infinite width parallel textures*, Tribology International, 43 (2010), pp. 1551–1565, <https://doi.org/10.1016/j.triboint.2010.02.016>.
- [13] S. SEN AND J. C. KALITA, *A 4OEC scheme for the biharmonic steady Navier–Stokes equations in non-rectangular domains*, Computer Physics Communications, 196 (2015), pp. 113–133, <https://doi.org/10.1016/j.cpc.2015.05.024>.
- [14] S.-H. SHYU AND W.-C. HSU, *A numerical study on the negligibility of cross-film pressure variation in infinitely wide plane slider bearing, Rayleigh step bearing and micro-grooved parallel slider bearing*, Mechanical Sciences, 137 (2018), pp. 315–323, <https://doi.org/10.1016/j.ijmecsci.2018.01.031>.
- [15] S. TAKEUCHI AND J. GU, *Extended Reynolds lubrication model for incompressible Newtonian fluid*, Physical Review Fluids, 4 (2019), <https://doi.org/10.1103/PhysRevFluids.4.114101>.